Journal of Power Sources 208 (2012) 1–8

Contents lists available at SciVerse ScienceDirect

Journal of Power Sources

journal homepage: www.elsevier.com/locate/jpowsour

One-step synthesis of branched sulfur/polypyrrole nanocomposite cathode for lithium rechargeable batteries

Yongguang Zhang[a], Zhumabay Bakenov[b], Yan Zhao[a], Aishuak Konarov[a], The Nam Long Doan[a], Muhammad Malik[a], Todd Paron[a], P. Chen[a,*]

[a] Department of Chemical Engineering, University of Waterloo, 200 University Avenue West, Waterloo, Ontario, N2L3G1 Canada
[b] School of Engineering, Nazarbayev University, 53 Kabanbay Batyr Avenue, Astana 010000, Kazakhstan

ARTICLE INFO

Article history:
Received 20 December 2011
Received in revised form 2 February 2012
Accepted 2 February 2012
Available online 10 February 2012

Keywords:
Lithium–sulfur battery
Sulfur cathode for lithium batteries
Sulfur/polypyrrole composite
Conducting sulfur composite

ABSTRACT

A nanostructured sulfur/polypyrrole binary composite was prepared by a simple one-step ballmilling without heat-treatment. High resolution transmission and scanning electronic microscopy showed the formation of a highly developed branched structure consisting of polypyrrole with uniform sulfur coating on its surface. Exclusion of heat-treatment in the composite preparation avoided the sulfur loss; the composite contained 65 wt% of sulfur. AC impedance spectroscopy data exhibited remarkable reduction in charge transfer resistance of the composite compared with pristine sulfur. This may be due to the high conductivity and large surface area of polypyrrole. This charge transfer enhancement led to the electrochemical performance improvement of the composite cathode, delivering first discharge capacity of 1320 mAh g^{-1}.

1. Introduction

Lithium-ion batteries are leading power sources for various portable applications, such as laptops, cellular phones and even hybrid-electric and electric cars, due to their high energy density, stable and long charge–discharge cycle life. However, the toxicity and safety issues of cobalt based cathodes in commercial lithium-ion batteries are limiting their wide applications. Recently, cheaper and less toxic $LiMn_2O_4$ and $LiFePO_4$ cathodes have been successfully developed [1–3]. Other potential cathode candidates, such as $LiMnPO_4$ [4,5] and $LiCoPO_4$ [6,7] have also received interest. The theoretical capacities of these materials (equal or less than 170 mAh g^{-1}) are however relatively low, and cannot fully satisfy the application requirements for electric cars and large scale energy storage, such as wind or solar energy storage. Alternative cathode materials with high energy density and of low cost are thus needed. The lithium/sulfur (Li/S) system is one of the more promising candidates, due to its low cost, environmental friendliness and large theoretical capacity at 1672 mAh g^{-1} of sulfur (S) [8]. However, the insulating nature of S and solubility of polysulfides as discharge products restrict the practical application of Li/S battery. The cathode electronic conductivity could be enhanced by preparing a composite of S and conductive materials, such as carbon and conducting polymers. Those conductive materials should preferably have high specific surface area and porous structure in order to absorb and contain polysulfides. Moreover, the structure flexibility is important to accommodate large volume change during charge–discharge. Recently, active carbon [8], mesoporous carbon [9,10], multiwalled carbon nanotube [11,12] and conductive polymers [13–17] have been used for this purpose. Among them, polypyrrole (PPy) is a conductive polymer with a conductivity from a few mS cm^{-1} to 1–100 S cm^{-1} (depending on its morphology and the synthesis technique) and a high absorption ability [18–20]; it has been used in Li/S batteries [15–17]. It was shown that along with the conductivity improvement, the PPy acts as a distribution agent favoring homogeneous sulfur distribution in the composite [16]. Sun et al. [16] synthesized a nanowired sulfur/PPy (S/PPy) composite with a network structure via a heat treatment method. The specific discharge capacities of 1222 mAh g^{-1} and 570 mAh g^{-1} were delivered in the first and 20th cycles, respectively. Liang et al. [17] reported that S penetrates into the tubular PPy fibers by the capillary forces during a co-heating process. The composite containing 30 wt% S retained a specific capacity of around 650 mAh g^{-1} over 80 cycles. Although the combination of S with PPy showed great improvement in electrochemical performance in comparison with S powder, the heat treatment step in these studies makes the process more complicated, time and energy consuming. Moreover, S was evaporated and lost during the heat treatment steps [17]. Therefore, the development of novel techniques to prepare S/PPy composites without heat treatment is useful.

In this study, we report on preparation of a novel branched, nanostructured S/PPy composite via a single-step ballmilling,

* Corresponding author. Tel.: +1 519 888 4567x35586; fax: +1 519 888 4347.
E-mail address: p4chen@uwaterloo.ca (P. Chen).

0378-7753/$ – see front matter © 2012 Elsevier B.V. All rights reserved.
doi:10.1016/j.jpowsour.2012.02.006

without heat treatment, and investigation of its physical and electrochemical properties as a cathode for lithium secondary batteries.

2. Experimental

2.1. Material synthesis

Polypyrrole was synthesized as described in Wu et al.'s work [18], with some modifications in the preparation procedure. 12.4 g cetyltrimethylammonium bromide (CTAB) (Sigma, ≥99.9% purity) was dissolved in 0.75 L deionized water, and then 0.015 L of pyrrole monomer (Aldrich, 98% purity) was added into the CTAB solution, stirred for 3 h. Subsequently, 0.045 L aqueous solution of 5.1 g ammonium persulfate (Sigma–Aldrich, 98% purity) was added, as an oxidizing agent, to initiate the polymerization, and the solution was stirred for 24 h. All synthesis procedures were carried out in a temperature range between 0 and 5 °C. The final precipitate of PPy was separated via filtration, thoroughly washed with deionized water and ethanol, and then vacuum dried overnight at 70 °C. To make S/PPy composite, PPy was mixed with S (Sigma–Aldrich, 100-mesh particle size powder) in the weight ratio PPy:S = 1:2, by ballmilling for 3 h at 600 rpm.

2.2. Material characterization

The chemical transformation of the composite during the preparation process was investigated by Fourier Transform Infrared Spectroscopy (FTIR, 520, Nicolet). The crystalline phases of the sample were determined by X-ray diffraction (XRD, D8 Discover, Bruker) equipped with Cu Kα radiation. The composite surface morphology was examined by field emission scanning electron microscopy (FE-SEM, Leo-1530, Zeiss). The interior structure of S/PPy composite was observed using transmission electron microscopy (TEM, CM10, Philips) at 60 kV and high resolution transmission electron microscopy (HRTEM, FEI TITAN 80-300) equipped with Energy Dispersive Spectroscopy (EDS). The PPy nanowires diameter distribution, the calculation of the geometric mean diameter $d_{g,p}$ and the geometric standard deviation σ_g were done via a random sampling of nanowires from the FE-SEM images, as described elsewhere [21]. The specific surface area was determined by the Brunauer–Emmet–Teller method (BET, ASAP 2020, Micromeritics). The S content in S/PPy composite was determined using chemical analysis (CHNS, Vario Micro Cube, Elementar).

2.3. Electrochemical measurements

The electrochemical performance of S/PPy composite samples was investigated using coin-type cells (CR2032). The cell was composed of lithium metal anode and S/PPy cathode separated by a microporous polypropylene separator soaked in 1 mol L^{-1} solution of lithium bistrifluoromethanesulfonamide (LiTFSI) (Aldrich, 96% purity) in tetraethylene glycol dimethyl ether (Aldrich, 99% purity) electrolyte. The composite cathode was prepared by mixing 80 wt% S/PPy, 10 wt% polyvinylidene fluoride (PVdF) (Kynar, HSV900) as a binder and 10 wt% acetylene black (MTI, 99.5% purity) conducting agent in 1-methyl-2-pyrrolidinone (NMP, Sigma–Aldrich, ≥99.5% purity). The sulfur cathode, with a weight ratio S:AB:PVdF = 6:3:1, and the PPy cathode with the composition PPy:AB:PVdF = 6:3:1 were also prepared in the same way as the S/PPy composite cathode. The resultant slurry in NMP was spread onto a circular piece of nickel foam (MTI, ≥99% purity) with 1 cm in diameter. After drying in a vacuum oven for 12 h at 60 °C, the cathode was pressed at 8 MPa by a hydraulic press in order to achieve good contact between the active material and nickel foam. The electrodes were prepared to make their weight and thickness the same by precise weighing, pressing and controlling its geometry. The sulfur loading in each electrode is about 4 mg cm^{-2}. The PPy and S/PPy samples were pelletized using a hydraulic press and used for the specific conductivity estimation, sandwiched between two parallel stainless steel plates by means AC impedance measurement (VM3, Biologic). The coin cells were assembled in a Braun glove box filled with high purity argon (99.9995% purity). The cells were tested galvanostatically on a multichannel battery tester (BT-2000, Arbin Instruments) between 1 and 3 V vs. Li^+/Li electrode at a current density of 100 mA g^{-1}. Applied currents and specific capacities were calculated on the basis of the weight of S in the cathode.

Cyclic voltammetry (CV) and AC electrochemical impedance spectroscopy (EIS) were performed with a potentiostat (VMP3, Biologic). CV was conducted between 1 and 3 V vs. Li^+/Li at a scanning rate of 0.1 mV s^{-1}. The frequency of EIS was varied from 1 MHz to 1 Hz with applied voltage amplitude of 10 mV. All electrochemical measurements were performed at room temperature.

3. Results and discussion

3.1. Properties of PPy nanowires and S/PPy composite

From the FTIR spectrum of prepared PPy shown in Fig. 1a, it could be seen that the characteristic bands of the PPy are consistent with the literature data [16,17,22,23]. The pyrrole ring fundamental vibrations are at 1545 cm^{-1} and 1458 cm^{-1}, the =C—H in-plane vibrations are at 1291 cm^{-1} and 1043 cm^{-1}, and the C—N stretching vibration is at 1175 cm^{-1}. Therefore, it could be concluded that the PPy structure could be successfully obtained via the chemical

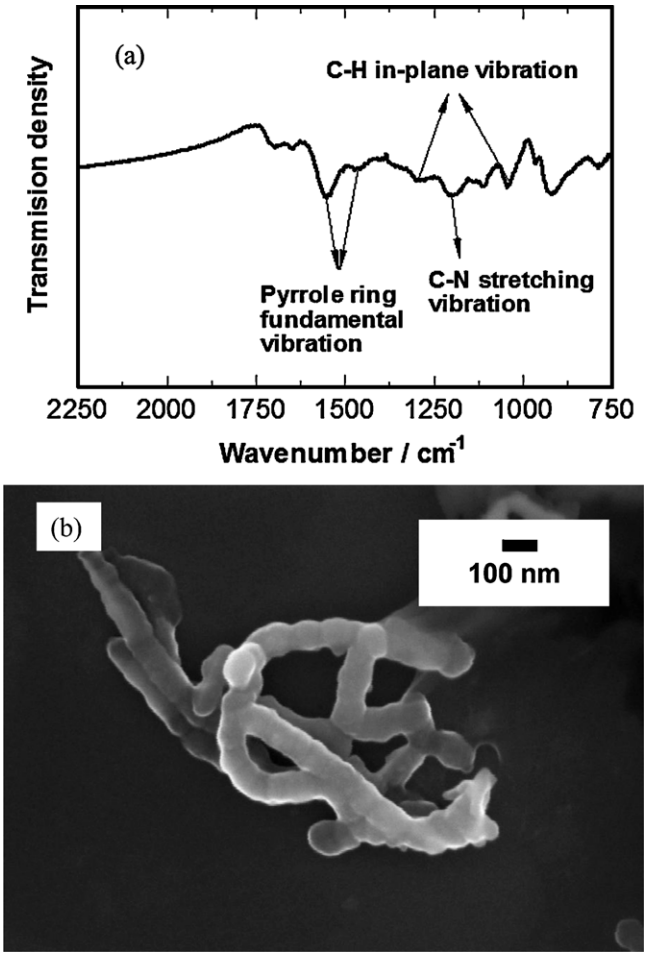

Fig. 1. (a) FTIR spectrum and (b) SEM image of as prepared PPy nanowires prepared by the polymerization of pyrrole monomer in CTAB solution.

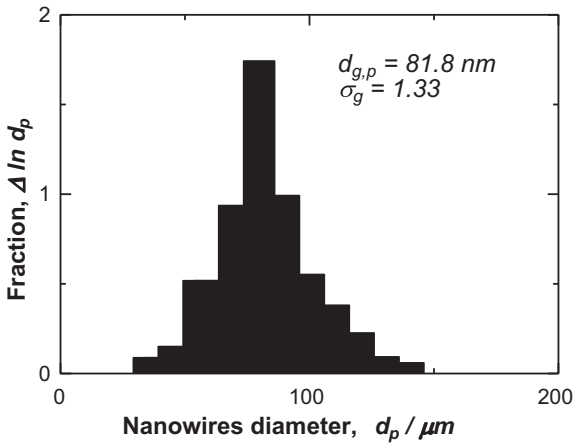

Fig. 2. Distribution of the diameters of as prepared PPy nanowires prepared by the polymerization of pyrrole monomer in CTAB solution.

polymerization method. The morphology of this material was observed by SEM as given in Fig. 1b. One can see that in the presence of CTAB, polypyrrole was formed as separated nanowires. It was reported that CTAB can form rod-like micelles when organic nanoparticles solubilize into their hydrocarbon core [24]; these rods further direct the fibers growth like a template. It can be seen from Fig. 1b that PPy nanowires prepared in the present study are less than 100 nm in diameter. Fig. 2 presents the PPy nanowires diameter distribution obtained from the SEM observation data [21]. PPy nanowires have uniform diameter distribution with a geometric mean diameter of $d_{g,p}$ = 81.3 nm and a geometric standard deviation of σ_g = 1.33.

The XRD patterns of pure S, pure PPy and S/PPy composite are shown in Fig. 3. One can see that while PPy was amorphous, the XRD patterns of the S used in this work exhibited *Fddd* orthorhombic structure for elemental sulfur. In comparison with S, the S/PPy composite showed sharp peaks of S with reduced peak intensity. On the other hand, no peak shift could be observed, which could be an indication of the absence of phase transformations due to ballmilling, and the sulfur crystal structure remained in the S/PPy composite. However, the XRD peak intensity reduction may indicate partial absorption of melted sulfur, during ballmilling, into the porous structure of PPy, since ballmilling generates heat and the temperature increase over the melting point of sulfur.

In this work, the conductive S/PPy composite was obtained via one-step high speed ballmilling of the mixture of sulfur and PPy, and no additional heat treatment was applied in the preparation process. Chemical analysis has shown that the sulfur content in the S/PPy composite was about 65 wt%, i.e., there is no significant sulfur loss when the composite was prepared by the current method. This resulted in about 52 wt% of sulfur in the composite cathode used in the test cell.

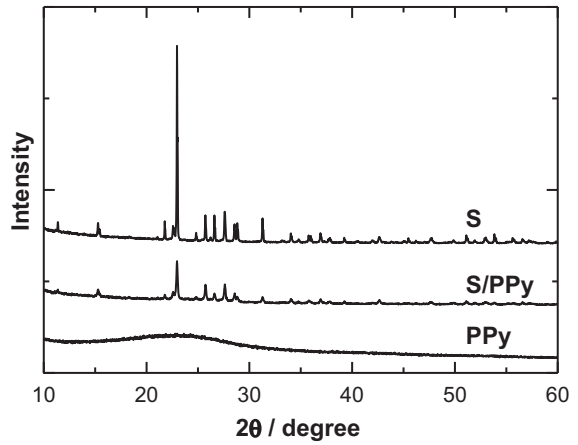

Fig. 3. XRD patterns of S, PPy and S/PPy composite samples.

Fig. 4 shows HRTEM images of as prepared PPy. At a higher magnification (Fig. 4a), no obvious lattice fringes can be observed, and PPy has the amorphous structure, which is consistent with XRD results. The EDS carbon mapping of PPy (Fig. 4c and 2d) shows homogeneous carbon distribution.

The TEM data presented in Fig. 5a shows that the S/PPy composite prepared via the present technique has a well-developed branched structure. HRTEM (Fig. 5b) of S/PPy composite shows the crystal lattice strips in the outer part of the composites nanostructure with a measured neighboring interlayer distance of 0.38 nm, which corresponds to the (2, 2, 2) crystal plane of S. This suggestion is in good agreement with the XRD results that the S/PPy composite remained the well-distinguished peaks of S. The inner part of the S/PPy composite is less crystalline (Fig. 5d) which is due to the amorphous PPy nanowires. Fig. 5e–g presents the EDS mapping of the S/PPy composite. One can see that sulfur is homogeneously distributed over the PPy nanowired substrate. This well-developed branched structure of S/PPy with homogeneous distribution of sulfur in it enhances the contact of sulfur to conductive PPy, which is important for the electrochemical performance of the composite cathode material.

Specific surface area of the as-prepared PPy was 129.8 $m^2\ g^{-1}$ with the pore volume of 0.55 $cm^3\ g^{-1}$. After mixing with sulfur, the specific surface area of S/PPy was only 4.4 $m^2\ g^{-1}$ with the pore volume of 0.052 $cm^3\ g^{-1}$. This remarkable specific surface area and pore size reduction could be mainly due to deposition of a large amount of sulfur into the pores and surface of PPy. The formation of the S/PPy composite with homogeneous sulfur deposition on the conductive PPy surface may drastically improve the conductivity of the composite cathode [23], which is important for the sulfur utilization and increase of the sulfur cathode capacity. Furthermore, the branched nanostructure of S/PPy could accommodate the volume change of the composite during charge and discharge [25] and improve the cyclability of the composite cathode.

A high S content cathode is desirable to construct a high energy density battery. Exclusion of the heat treatment from the synthetic route for the S/PPy composite along with saving energy and simplifying the preparation process prevents the sulfur loss due to its sublimation. This also prevents the generation of toxic volatile sulfur compounds at high temperature conditions; therefore, the preparation technique developed in this work could be more preferable than the conventional prolonged multi-step and high temperature techniques for preparation of conductive S-containing composites.

3.2. Electrochemical properties of S/PPy composite cathode material

The CV curves are shown in Fig. 6 for S, PPy, and S/PPy composite, used as a cathode active material in the lithium half-cell. One can see that for the pure S cathode, one broad reduction peak was observed about 1.5 V vs. Li^+/Li, and the electrochemical processes are slow and poorly reversible. It can also be seen that PPy is electrochemically inactive within the studied potential region and there are no noticeable electrochemical processes observed in the pure PPy cathode. In the case of the S/PPy composite cathode, two pairs of complex reversible redox peaks were clearly observed around 2 and 2.5 V, which is possible due to the multi-step electrochemical reactions of S with Li^+ [26,27]. The CV data reveals that PPy improves the electrochemical kinetics of S, which could be due to the electronic conductivity enhancement of the composite cathode by the

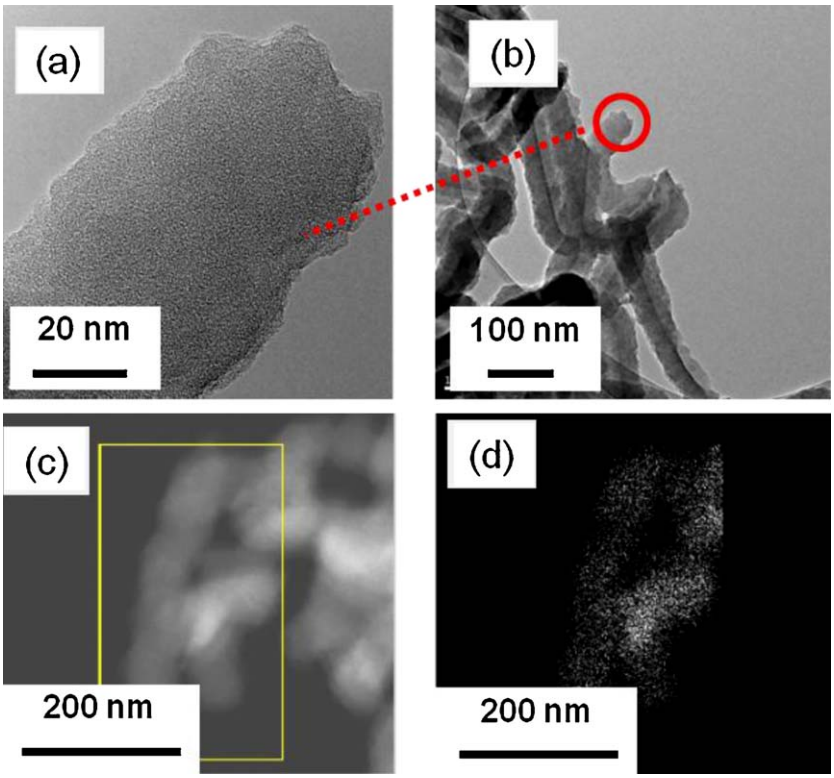

Fig. 4. HRTEM images of PPy samples at different magnifications and EDS mapping showing distribution of carbon.

addition of conductive PPy [16]. The specific conductivity (σ) of the nanowired PPy synthesized in this work and that of the binary S/PPy composite was estimated by means of AC impedance technique using the pellets made from pure PPy and S/PPy samples. While the pure sulfur cathode prepared as described in the experimental part (S:AB:PVdF = 6:3:1 by weight) exhibited almost insulating properties ($\sigma < 10^{-10}$ S cm^{-1}), the conductivity of pure PPy with no additives was estimated as 95 S cm^{-1}, which is comparable with the data obtained for PPy by a four-probe DC technique [16,18,19]. The specific conductivity of the S/PPy composite prepared in this work (weight ratio PPy:S = 1:2) was about 3×10^{-5} S cm^{-1}, i.e., the conductivity of sulfur has been improved by more than five orders of magnitude by adding the nanowired PPy prepared in this work.

The initial profiles of galvanostatic charge–discharge tests of the S/PPy cathode are shown in Fig. 7. It can be seen that two main plateaus appear in the potential profiles, which could be attributed to two main electrochemical reactions taking place at sulfur cathode upon cycling in Li/S battery. The results are in good agreement with the CV data. The first electrochemical reaction is presented by a short discharge plateau about 2.5 V and related to the formation of higher-order lithium polysulfides (Li_2S_n, $n \geq 4$), which are soluble in the liquid electrolyte [26–28]. The following prolonged plateau around 2.0 V in the discharge profiles reflects the following electrochemical transition of the polysulfides to lithium sulfide Li_2S, and this reaction kinetics is slower than that of the polysulfide formation [26–29]. It could be seen that while the 2 V discharge plateaus had no remarkable difference between the first and third cycles, the higher voltage plateau diminishes and almost disappears after a few cycles. This could be due to the activation of the composite cathode upon initial cycles, and achieving a steady state for the polysulfide formation. It can be seen here that a discharge capacity of 1050 mAh g^{-1} was obtained at the third cycle, the 2.4 V plateau is short, and the system's discharge capacity mainly depends on the 2 V plateau.

The S/PPy composite cathode performance was remarkably enhanced compared with that of the pure S cathode as shown in Fig. 8. Although the cathode cyclability was improved by the PPy additive, more remarkable enhancement has been observed in the sulfur utilization in the S/PPy composite compared with pure sulfur counterpart. This lead to a high discharge capacity of the composite cathode, which stabilized after 25 cycles at about 600 mAh g^{-1} and retained about 500 mAh g^{-1} after 40 cycles. The performance improvement could be attributed to the multiple effects of the PPy additive such as conductivity and sulfur distribution, and an active absorber for the reaction products [16]. The sulfur particles were evenly distributed over the highly branched nanowired PPy and were connected by this conductive network, and both factors were positively affecting the sulfur utilization in the composite material. Moreover, the highly developed surface and absorbing ability of the nanowired PPy could accommodate the large volume change of S on the PPy branched structure and the absorption of polysulfides into the pores of PPy. This phenomenon could enhance the mechanical adhesion sulfur with the conductive PPy network, maintaining the higher sulfur utilization upon cycling compared with the pure sulfur cathode. Although the sulfur dissolution was drastically suppressed by the PPy additive and was more than three times lower than that for the pure sulfur cathode (chemical analysis data, not shown), it could contribute to a gradual capacity fading of the composite cathode. Another reason for the S/PPy composite cathode degradation could be the agglomeration of S particles upon prolonged cycling, although we could not observe remarkable sulfur distribution change over a few tens of charge–discharge cycles. In contrast, the S cathode exhibited very low discharge capacity due to high resistance of sulfur and consequent low sulfur utilization, and its capacity quickly decreased with cycling due to the accelerated electrochemical dissolution of sulfur. The cell with pure sulfur cathode had a discharge capacity of only about 110 mAh g^{-1} at the 40th cycle. The poor cyclability of the S cathode could be also attributed

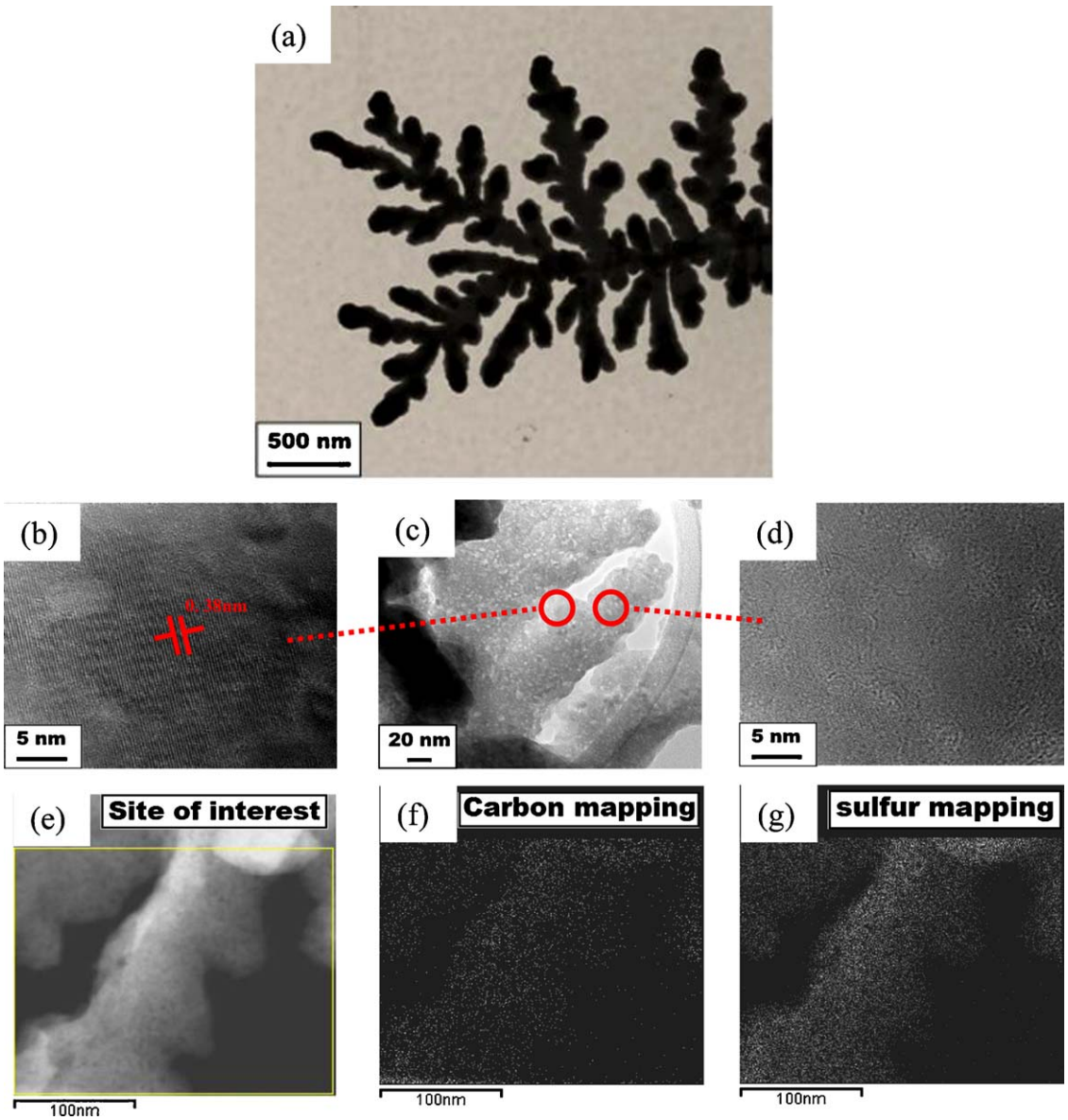

Fig. 5. (a) TEM and (b–d) HRTEM images of S/PPy composite at different magnifications. The crystalline phase of S could be observed in (b) and amorphous phase of PPy could be identified in (d), which are located on the surface and in the core of the branched S/PPy composite structure as shown in (c). Moreover, the (f) carbon mapping and (g) sulfur mapping of the (e) TEM image showing the uniform distribution of those elements.

to the mechanical destruction of the cathode caused by the inherent periodic volume expansion/shrinkage upon cycling.

The sulfur shuttle mechanism [30] is a typical phenomenon in lithium–sulfur batteries, resulting in imperfect charging and decrease of discharge capacity, which leads to a low coulombic efficiency of the cell. Fig. 9 presents the coulombic efficiency vs. cycle number for the S/PPy lithium cell. The cells exhibited a high coulombic efficiency of 97% at the initial cycle. However, the coulombic efficiency decreases to 89% in the second cycle and 80% in the 5th cycle. In the first cycle, the sulfur still evenly distributed on the surface of branched PPy, and this provides a high level of the cathode reversibility because of good electronic conductivity. However, as described in the previous paragraph, both the sulfur shuttle/dissolution and the sulfur particle agglomeration could result in the reversible capacity loss. Therefore, the coulombic efficiency of the battery gradually reduces for several consequent cycles. Further cycling leads to the coulombic efficiency increase, which could be due to the good contact of the remaining S with porous PPy network, allowing improved reversibility of

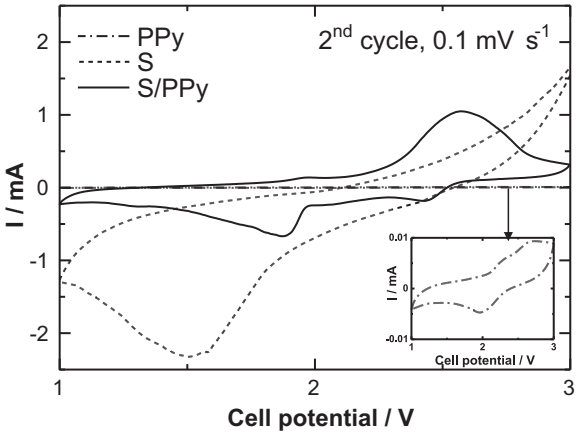

Fig. 6. CV profiles of lithium cells with S, PPy and S/PPy composite cathodes. The potential sweep rate is 0.1 mV.

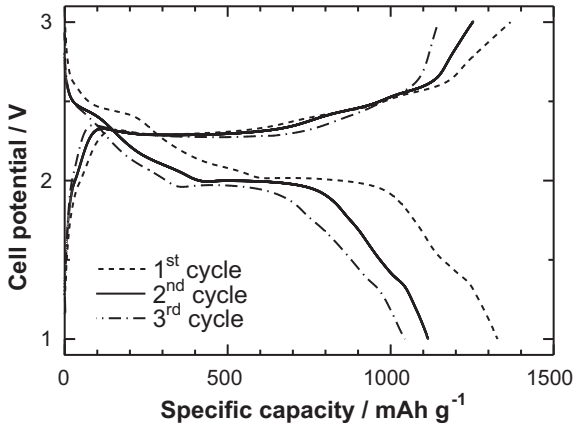

Fig. 7. Charge/discharge profiles of lithium cell with S/PPy composite cathode at a current density of 100 mA g^{-1}.

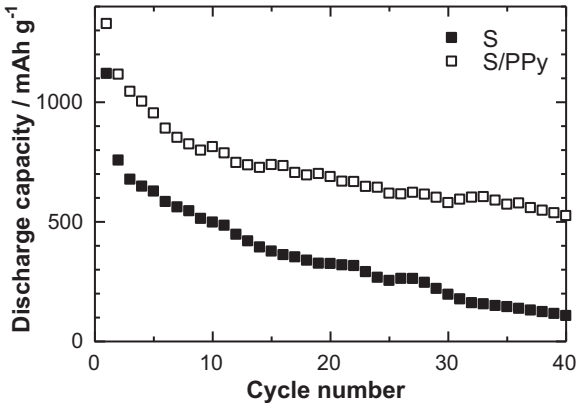

Fig. 8. Cycle performance of lithium cells with S and S/PPy composite cathodes at a current density of 100 mA g^{-1}.

the system. The coulombic efficiency reaches 96% after around 40 cycles, i.e., the shuttle mechanism effect is reduced upon prolonged cycling. Therefore the capacity fading of S/PPy composite cathode upon prolonged cycling could be mostly due to the sulfur particles agglomeration and to the lesser extent from the shuttle effect.

The enhancement of cathode conductivity could be confirmed by a comparison of EIS data of the cells with S and S/PPy cathodes as given in Fig. 10 for fresh cells. Both cathodes exhibited the Nyquist plots comprising of a compressed semicircle in the high

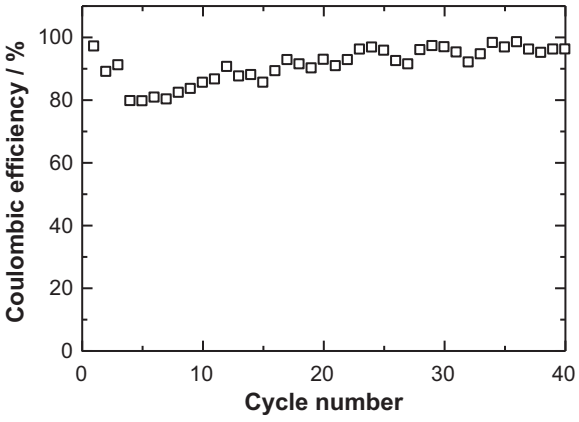

Fig. 9. Coulombic efficiency of lithium cells with S/PPy composite cathodes vs. cycle number at a current density of 100 mA g^{-1}.

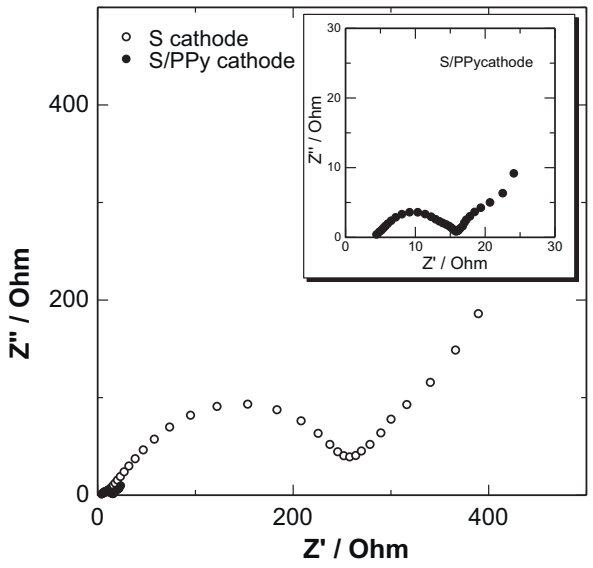

Fig. 10. EIS plots of lithium cells with S and S/PPy composite cathodes in the frequency range of 0.01–10^6 Hz.

to medium frequency range and an inclined line in the lower frequency range, which could be represented by a Randles equivalent circuit [31]. For the composite electrodes containing highly conductive carbon, the depressed semicircle could be related to the interfacial charge transfer [32–34]. The inclined line in the lower frequency represented the Warburg impedance, associated with lithium-ion diffusion in the electrode particles. A much smaller high-to-medium frequency semicircle can be seen in the S/PPy electrode EIS spectra compared with that of the sulfur cathode. This indicates a significant decrease in charge transfer resistance in the S/PPy composite compared with the pristine S electrode. This may be due to the high conductive polypyrrole additive. This charge transfer enhancement leads to the electrochemical performance improvement of the composite cathode.

The studied S/PPy composites consist of multiple interfaces and phase boundaries, and although the complete impedance analysis is complicated, some simple suggestions can be made using the EIS data [31,32]. Fig. 11a represents the data on the EIS development in S/PPy based lithium half-cell upon cycling. It can be seen that within the first few charge–discharge cycles the Nyquist plot of the cell has transformed from a single compressed semicircle type to a more complicated plot consisting of a combination of an inclined line in the high frequency part, two compressed semicircles in the high to medium frequency range followed by an inclined line of the Warburg impedance. Further cycling leads to the total impedance growth and merging of two medium frequency semicircles into a single Randles type impedance plot, which represents the system during the following charge–discharge. These transformations indicate a complex character of the interfacial processes taking place during the initial charge–discharge cycles, including the formation of solid electrolyte interface (SEI), which protects the cathode from further decomposition. The total impedance growth could be attributed to possible agglomeration of the sulfur particles and loss of its contact with the conducting PPy network. The equivalent circuit fitting was applied to the experimental EIS data for the first 10 charge–discharge cycles using EC-Lab Software (Bio-Logic Instruments, V10.19). Fig. 11b represents the fitting results and the inset shows the best fitting equivalent circuit, which could be represented as follows:

$$L1 + R1 + Q2/R2/(Q3 + R3)/(R4 + W4) \quad (1)$$

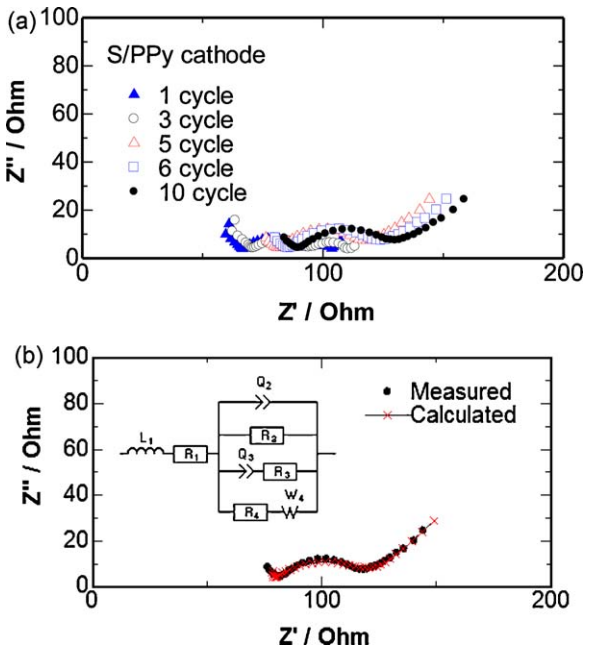

Fig. 11. (a) EIS development in lithium cell with S/PPy composite cathode and (b) equivalent circuit fitting of the experimental EIS data (inset shows the obtained equivalent circuit).

where L1 is an inductor element, R1–R4 represent the ohmic resistance at the interfaces, Q2 and Q3 are the constant phase elements responsible for the double layer capacitance component of the system impedance, and W4 is the Warburg impedance. One can see that the system could be well fitted (fitting goodness close to 1) with a multi-component equivalent circuit with a complicity of the quantitative interpretation. The part of this circuit including the part Q2/R2/(Q3 + R3)/(R4 + W4) connected in parallel and the Warburg impedance could be attributed to the complex impedance of the solid/solid and solid/liquid interfaces and the bulk diffusion resistance of the S/PPy composite cathode. Further detailed investigation of the complex impedance behavior of the system is under progress and out of scope of this paper.

The S/PPy composite was prepared in this work via a simple one-step technique and no heat-treatment was used. This can be considered as an economic and environmentally friendly approach because exclusion of heating prevents the sulfur loss and the formation of harmful sulfur compounds during the synthesis. The material exhibits enhanced electrochemical performance in a lithium cell with liquid electrolyte, which is comparable with that of the sulfur-containing cathodes prepared via complicated techniques using expensive conductive carbons [8–10]. Therefore, the current preparation technique could be considered a promising approach to prepare high performance sulfur cathodes for lithium battery application. Further investigations under progress aimed to improve cycling performance of the composite cathode in our laboratory.

4. Conclusions

The polypyrrole nanowires were prepared via chemical polymerization of pyrrole. These nanowires were used as a conductive matrix to prepare a branched binary sulfur/PPy nanocomposite by a simple, one-step ballmilling, without any heat treatment. The S/PPy composite consisted of the branched conductive PPy matrix uniformly coated with S. The use of conductive PPy matrix has improved the electrochemical performance of the composite cathode in lithium battery via the enhanced charge transfer in the electrode. Furthermore, the branched structure of the nanocomposite and high porosity of the PPy matrix could accommodate the mechanical stresses induced by the volume changes upon charge–discharge and hinder the polysulfide dissolution. The S/PPy composite cathode exhibited enhanced electrochemical performance and allowed stable cycling of the lithium half-cell with a high sulfur utilization expressed in high discharge capacity and coulombic efficiency of the Li/S rechargeable battery. The major role of the capacity decay upon cycling was attributed to possible agglomeration of the S particles leading to the loss of connection between sulfur and conductive PPy network and increasing the composite resistance. The EIS impedance studies revealed the total impedance growth during cycling, which could be caused mainly by the S agglomeration. One-step preparation technique developed in this work allows the preparation of high performance two-component S/PPy composite cathode with three-dimensional branched structure.

Acknowledgements

This research was financially supported by Positec, Natural Sciences and Engineering Research Council of Canada (NSERC), Canadian Foundation for Innovation (CFI) and the Canada Research Chairs (CRC). The EM research described in this paper was performed at the Canadian Centre for Electron Microscopy at McMaster University, which is supported by NSERC and other government agencies. One of the authors (Y.Z.) thanks the China Scholarship Council for Study Abroad Scholarship.

References

[1] D. Song, H. Ikuta, T. Uchida, M. Wakihara, Solid State Ionics 117 (1999) 151.
[2] Z. Bakenov, I. Taniguchi, Solid State Ionics 176 (2005) 1027–1034.
[3] B. Kang, G. Ceder, Nature 458 (2009) 190–193.
[4] S.K. Martha, B. Markovsky, J. Grinblat, Y. Gofer, O. Haik, E. Zinigrad, D. Aurbach, T. Drezen, D. Wang, G. Deghenghi, I. Exnar, J. Electrochem. Soc. 156 (2009) A541.
[5] G. Li, H. Azuma, M. Tohda, Electrochem. Solid-State Lett. 5 (2002) A135–A137.
[6] H.H. Li, J. Jin, J.P. Wei, Z. Zhou, J. Yan, Electrochem. Commun. 11 (2009) 95–98.
[7] T.N.L. Doan, I. Taniguchi, J. Power Sources 196 (2011) 5679–5684.
[8] J.L. Wang, J. Yang, J.Y. Xie, N.X. Xu, Y. Li, Electrochem. Commun. 4 (2002) 499–502.
[9] X.L. Ji, K.T. Lee, L.F. Nazar, Nat. Mater. 8 (2009) 500–506.
[10] J. Wang, S.Y. Chew, Z.W. Zhao, S. Ashraf, D. Wexler, J. Chen, S.H. Ng, S.L. Chou, H.K. Liu, Carbon 46 (2008) 229–235.
[11] S.C. Han, M.S. Song, H. Lee, H.S. Kim, H.J. Ahn, J.Y. Lee, J. Electrochem. Soc. 150 (2003) A889–A893.
[12] L.X. Yuan, H.P. Yuan, X.P. Qiu, L.Q. Chen, W.T. Zhu, J. Power Sources 189 (2009) 1141–1146.
[13] J.L. Wang, J. Yang, C.R. Wan, K. Du, J.Y. Xie, N.X. Xu, Adv. Funct. Mater. 13 (2003) 487–492.
[14] X.G. Yu, J.Y. Xie, J. Yang, K. Wang, J. Power Sources 132 (2004) 181–186.
[15] J. Wang, J. Chen, K. Konstantinov, L. Zhao, S.H. Ng, G.X. Wang, Z.P. Guo, H.K. Liu, Electrochim. Acta 51 (2006) 4634–4638.
[16] M.M. Sun, S.C. Zhang, T. Jiang, L. Zhang, J.H. Yu, Electrochem. Commun. 10 (2008) 1819–1822.
[17] X. Liang, Y. Liu, Z.Y. Wen, L.Z. Huang, X.Y. Wang, H. Zhang, J. Power Sources 196 (2011) 6951–6955.
[18] A. Wu, H. Kolla, S.K. Manohar, Macromolecules 38 (2005) 7873–7875.
[19] E.A. Song, W.G. Jung, D.W. Ihm, J.Y. Kim, Bull. Korean Chem. Soc. 30 (2009) 1009–1011.
[20] J.Y. Kim, J.T. Kim, E.A. Song, Y.K. Min, H. Hamaguchi, Macromolecules 41 (2008) 2886–2889.
[21] I. Taniguchi, Mater. Chem. Phys. 92 (2005) 172–179.
[22] J.T. Lei, W.B. Liang, C.R. Martin, Synth. Met. 48 (1992) 301–312.
[23] K. Cheah, M. Forsyth, V.T. Truong, Synth. Met. 94 (1998) 215–219.
[24] H.B. Fu, D.B. Xiao, J.N. Yao, G.Q. Yang, Angew. Chem. Int. Ed. 42 (2003) 2883–2886.
[25] X. He, J. Ren, L. Wang, W. Pu, C. Jiang, C. Wan, J. Power Sources 190 (2009) 154–156.
[26] D. Marmorstein, T.H. Yu, K.A. Striebel, F.R. McLarnon, J. Hou, E.J. Cairns, J. Power Sources 89 (2000) 219–226.
[27] D.H. Han, B.S. Kim, S.J. Choi, Y. Jung, J. Kwak, S.M. Park, J. Electrochem. Soc. 151 (2004) E283–E290.
[28] H. Yamin, A. Gorenshtain, J. Penciner, Y. Sternberg, E. Peled, J. Electrochem. Soc. 135 (1988) 1045–1048.
[29] V.S. Kolosnitsyn, E.V. Karaseva, Russ. J. Electrochem. 44 (2008) 506–509.

[30] M.S. Song, S.C. Han, H.S. Kim, J.H. Kim, K.T. Kim, Y.M. Kang, H.J. Ahn, S.X. Dou, J.Y. Lee, J. Electrochem. Soc. 151 (2004) A791–A795.
[31] S.K. Martha, B. Markovsky, J. Grinblat, Y. Gofer, O. Haik, E. Zinigrad, D. Aurbach, T. Drezen, D. Wang, G. Deghenghi, J. Exnar, J. Electrochem. Soc. 156 (2009) A541–A552.
[32] Z. Bakenov, I. Taniguchi, J. Electrochem. Soc. 157 (2010) A430–A436.
[33] J.W. Choi, J.K. Kim, G. Cheruvally, J.H. Ahn, H.J. Ahn, K.W. Kim, Electrochim. Acta 52 (2007) 2075–2082.
[34] Y.J. Choi, Y.D. Chung, C.Y. Baek, K.W. Kim, H.J. Ahn, J.H. Ahn, J. Power Sources 184 (2008) 548–552.